

Hydrostatic stress and hydrostatic stress gradients in passivated copper interconnects

Ang, Derrick; Ramanujan, Raju V.

2006

Ang, D., & Ramanujan, R. V. (2006). Hydrostatic Stress and Hydrostatic Stress Gradients in Passivated Copper Interconnects. *Materials Science and Engineering: A*, 423, 157-165.

<https://hdl.handle.net/10356/94245>

<https://doi.org/10.1016/j.msea.2005.10.079>

© 2006 Elsevier. This is the author created version of a work that has been peer reviewed and accepted for publication by *Materials Science and Engineering: A*, Elsevier. It incorporates referee's comments but changes resulting from the publishing process, such as copyediting, structural formatting, may not be reflected in this document. The published version is available at: [DOI: <http://dx.doi.org/10.1016/j.msea.2005.10.079>].

Downloaded on 23 Aug 2022 02:29:03 SGT

Hydrostatic stress and hydrostatic stress gradients in passivated copper interconnects

D. Ang, R.V. Ramanujan

School of Materials Science and Engineering, Nanyang Technological University,

Blk N4.1, #01–18 Nanyang Avenue, Singapore 639798, Singapore

Tel.: +65 67904342; fax: +65 67909081.

E-mail address: ramanujan@ntu.edu.sg (R.V. Ramanujan).

Abstract

A numerical evaluation of the effects of geometrical factors on the hydrostatic stress and hydrostatic stress gradients in passivated copper interconnects was performed. These values were correlated with experimental values in the literature on the location of voids in the interconnect. Copper interconnects of aspect ratios between 0.1 and 10 were studied. Numerical work using the commercial ANSYS software and analytical work based on the Eshelby and Wikström models were performed. Comparison is made between the analytical, numerical and experimental results (obtained from the literature). It was found that for an interconnect with no pre-existing voids, maximum hydrostatic stress gradients occurred at the corners of the interconnects suggesting that void growth is most probable at the corners of the interconnect. The stress gradient within the interconnect with aspect ratio of 10 is about 10 times larger than that in interconnects of aspect ratios 0.1 and 1. This suggests that the narrowest interconnects are most likely to undergo voiding. This study found that it is insufficient to look only at the hydrostatic stress at the centre of the interconnect and that stress gradient also needs to be taken into consideration to assess reliability.

Keywords: Microelectronic reliability; Scaling effects; Stress voiding; Finite element method

1. Introduction

Copper was first introduced as a primary interconnect material in integrated circuits in 1997 by IBM due to its lower resistivity and better electromigration resistance than aluminium. As interconnect dimensions continue to scale down into deep submicron regime, stress-migration has become a major reliability issue. Stress-migration or stress-induced voiding was discovered in aluminium interconnects in semiconductor devices in 1981 [1]. It is a failure mechanism in which voids grow in the absence of applied voltage or imposed thermal gradient. There is an inherent tendency for voids to form in the aluminium interconnect because of the large difference in thermal expansion between aluminium and its more rigid passivation. Jones and Basehore showed that for narrow interconnects, the tensile stresses in the interconnects can be several times the yield strength [2]. Since then, many researchers have studied finite element modeling of passivated metal interconnects [3–17]. In the past, the location of voids has been correlated to the stress concentration locations [15–17].

The present work focused on an analytical and numerical study of the effect of aspect ratio scaling on the reliability of passivated copper interconnects. Specifically, the aim is to examine the relationship between stress and stress gradients on the location of the voids. In an earlier study [11], the absolute value of the width was chosen and the structure used was an aluminium-based structure. In the present study, the geometrical aspect ratio (height/width) and copper damascene structure were used. The interconnect was assumed to behave in either (i) elastic or (ii) elastic–perfectly plastic manner. The Wikström model [9], Eshelby inclusion model [18] and Eshelby inhomogeneity model [19] were used in the analytical study, whereas numerical results were obtained from a commercial finite element software, ANSYS. Unlike the Eshelby models, the Wikström model was developed to capture the interaction between neighbouring interconnects. The properties of the substrate and the interconnect width to interconnect spacing ratio are also taken into account in this model. In the Wikström model, the limiting case of a passivated isolated interconnect on a large substrate was used in this study. Interconnects with aspect ratio ranging from 0.1 to 10 were studied, and the height of the interconnects throughout the study was assumed to be 1 μm .

2. Finite element model

The finite element model of the copper damascene structure is as shown in Fig. 1. It consists of a 1 μm thick copper interconnect, a tantalum (Ta) barrier layer of thickness 20 nm for the bottom and 10 nm for the sidewall, and an etch stop layer (SiN) of thickness 50 nm. These thicknesses were held constant when studying the effect of aspect ratio scaling. The ratio of the total width of the model to the width of the interconnect is kept at 8:1. In this work, the directions along the interconnect width, thickness, and length are denoted by x -, y - and z -directions, respectively.

The interconnect was assumed to be very long and has both ends connected to other structures, hence it experiences no strain in the z -direction and a plane strain condition was used. It was also assumed that interactions between the interconnect and its neighbours are negligible. Due to symmetry, only one-half of the model was simulated. The boundary condition on the yz symmetry plane is zero x displacement. The Si substrate is also constrained at its base, i.e. no y displacement, the rest of the edges of the model are unconstrained. The whole assembly was assumed to be cooled from a stress-free state at 400 to 25 $^{\circ}\text{C}$.

In this study, SiO_2 , SiN, Ta and Si were modeled as temperature-dependent elastic materials while Cu was modeled as a temperature-dependent, elastic–plastic material. Materials properties as shown in Table 1 were taken from Refs. [2,6,20,21]. The yield strength of copper is assumed to be homogeneous and size-independent. The ANSYS finite element software was used to calculate the stresses. The hydrostatic stress referred to in the following sections is the stress at the centre of the interconnect. The hydrostatic stress, σ_{HS} , is defined as the average of σ_x , σ_y , and σ_z . The hydrostatic stress gradient is the ratio of the difference between the stress values of two consecutive nodes to the distance between the nodes. The magnitude of the hydrostatic stress gradient, $|\nabla \sigma_{\text{HS}}|$, is defined as

$$\sqrt{((d\sigma_{\text{HS}}/dx)^2 + (d\sigma_{\text{HS}}/dy))^2}.$$

3. Results and observations

3.1. Effect of aspect ratio

Fig. 2 shows the plot of the hydrostatic stress at the centre of the interconnect against aspect ratio for the case where the interconnect is assumed to behave in an elastic manner. This graph compares results from the three analytical models with numerical results. It can be observed that the Wikström model [9] and the Eshelby inclusion model yield a hydrostatic stress which is independent of aspect ratio, whereas the Eshelby inhomogeneity model yields an aspect ratio dependent hydrostatic stress as predicted by the numerical model. The rationale for the minimum point predicted by Eshelby inhomogeneity model and the numerical model has been provided in an earlier paper [11]. Briefly, the reason is that from aspect ratio of 10:1, the increase in σ_x is less than the decrease in σ_y . From aspect ratio of 1:0.1, the increase of σ_x is more than the decrease in σ_y . Since σ_z is proportional to the sum of σ_x and σ_y , hydrostatic stress is minimum at aspect ratio of 1. It is also noted that the Eshelby inclusion model predicts the highest hydrostatic stress. This is attributed to the assumption that the material properties (elastic modulus and Poisson ratio) of the dielectric material (SiO_2) are taken to be the same as that of the interconnect. From Table 1, it can be seen that in fact the elastic modulus of copper is about twice of that of SiO_2 .

Fig. 3 shows the plot of hydrostatic stress at the centre of the interconnect versus aspect ratio for the case where the interconnect is assumed to behave in an elastic–perfectly plastic manner. This plot includes results from Eshelby inhomogeneity model, numerical model and relevant experimental results from Marieb et al. [6] and Rhee et al. [10]. The existence of the maximum point as predicted by the analytical and numerical models is due to the larger stress relaxation experienced by interconnects with aspect ratios other than 1 [11]. There is good agreement between the analytical, numerical and experimental results as the predictions are within 50 MPa of the experimental values for aspect ratios around 1. It was also observed that Rhee’s results did not show a maximum at aspect ratio 1. This is due to the effect of periodicity of interconnects in the experimental work [22].

3.2. Hydrostatic stress and hydrostatic stress gradient contours

Figs. 4–6 show the hydrostatic stress contours for copper interconnects of aspect ratios 0.1, 1 and 10, respectively. These figures show that the maximum hydrostatic stresses are at the left and right interfaces, centre, and top and bottom of the interconnect for aspect ratios of 0.1, 1 and 10, respectively.

Figs. 7–12 show the plots of hydrostatic stress gradients for interconnects of aspect ratios 0.1, 1 and 10. It can be observed that maximum stress gradients occurred at the corners of the interconnects (corners are indicated by arrows in the figures).

4. Discussion

4.1. Hydrostatic stress and hydrostatic stress gradient contours

It was suggested in our earlier study [22] that the hydrostatic stress gradient could be a better predictor of void location than hydrostatic stress, as regions of high stress gradients coincide with void locations, whereas regions of high tensile stress do not. From a literature survey of void locations covering both aluminium [23–27] and

copper [28,29] interconnects with aspect ratios ranging from 0.1 to 5, it was found that voids appeared at the corners of the interconnects. This agrees with our results (Figs. 7–12) which clearly showed that maximum stress gradients indeed occurred at the corners of the interconnects.

There is concern that the same result may not be applicable for a periodic structure. An interconnect with aspect ratio 1 with interconnect width equals interconnect spacing was simulated. Fig. 13 shows that the minimum hydrostatic stress regions are at the corners of the interconnect, which is similar to the case of an isolated interconnect (Fig. 5). This means that for periodic structure, maximum stress gradients would also occur at the corners of the interconnect.

To understand the role of both maximum hydrostatic stress and stress gradients, let us take an interconnect of aspect ratio 1 as an illustration. Based on the maximum hydrostatic stress criterion, void nucleation is expected to occur at the centre of the interconnect (Fig. 5). Since the chemical potential is proportional to the negative of hydrostatic stress ($\mu \propto -\sigma_{HS}$) [30], atoms will move from the corners to the centre of the interconnect, i.e. vacancies will move and accumulate at the corners. However, for void growth ($J = -\mu \nabla \sigma$, where J is the atomic flux), stress gradients need to be present. From Figs. 9 and 10, we can see that significant stress gradients are present at the corners. Hence, for an interconnect with no pre-existing voids, void growth is most probable at the corners of the interconnect.

There is also concern regarding the use of plasticity in our modeling. A fully elastic model was performed on an isolated interconnect of aspect ratio 1. Figs. 14 and 15 show the hydrostatic stress and hydrostatic stress gradient contours, respectively. By similar reasoning as above, based on the maximum hydrostatic stress criterion, void nucleation is expected to occur at the corners of the interconnect (Fig. 14). Atoms will move from the centre to the corners of the interconnect, i.e. vacancies will move and accumulate at the centre. Fig. 15 shows that significant stress gradients are present at the corners. This suggests that void growth will occur away from the corners of the interconnect. This prediction is different from that of an elastic–plastic model, and more importantly, does not correlate with experimental observations.

Table 2 shows the magnitude of the stress gradients for interconnects of aspect ratios 0.1, 1 and 10. The stress gradient within the interconnect with aspect ratio of 10 is about 10 times larger than in interconnects of aspect ratios 0.1 and 1. This suggests that the narrowest interconnects are most likely to undergo voiding.

To assess the relative significance of lattice (D_l), grain boundary (D_{gb}) and interface (D_i) diffusivities in void formation, an estimate was made using the results from Fig. 3. For an interconnect of aspect ratio 2, the hydrostatic stress is 450 MPa. The following are assumed: time, $t = 20$ years and temperature, $T = 353$ K. D_l [31], D_{gb} [31] and D_i [32] are 2×10^{-34} , 6.2×10^{-21} and 2.5×10^{-20} m²/s, respectively. The corresponding characteristic lengths are $X_l = 8 \times 10^{-4}$ nm, $X_{gb} = 4$ μ m and $X_i = 8$ μ m. Considering the fact that the average grain size is 0.7 μ m [33], it is clear that both grain boundary diffusion and interface diffusion are significant in the case of copper. On the other hand, for aluminium, grain boundary diffusion is the dominant mechanism as it has a strong oxide layer which inhibits interface diffusion.

Having been aware of the important role of hydrostatic stress gradient, one should also bear in mind that plastic strain [34] and shear stresses across the interfaces [35] could also be important in determination of void locations.

5. Conclusions

Numerical work using commercial finite element package, ANSYS, and analytical work based on the Eshelby and Wikström models were performed to examine the effect of aspect ratio scaling on the hydrostatic stress and hydrostatic stress gradients in passivated metal interconnects. Copper interconnects of thickness 1 μm and linewidth ranging from 100 nm to 10 μm , corresponding to aspect ratios of 0.1:10, respectively, were studied. The following conclusions were drawn:

- (i) There is good agreement between the analytical, numerical and experimental results as the predictions are within 50 MPa of the experimental values for aspect ratios around 1.
- (ii) For an interconnect with no pre-existing voids, maximum hydrostatic stress gradients occurred at the corners of the interconnects and thus void growth is most probable at the corners of the interconnect.
- (iii) The stress gradient within the interconnect with aspect ratio of 10 is about 10 times larger than that in interconnects of aspect ratios 0.1 and 1. This suggests that the narrowest interconnects are most likely to undergo voiding.

In short, it is insufficient to look only at hydrostatic stress at the centre of the interconnect, both maximum hydrostatic stress and hydrostatic stress gradients need to be taken into consideration to assess reliability of interconnects.

Acknowledgement

The authors would like to thank Professor C.C. Wong for the helpful discussions during the course of this project.

References

- [1] P.A. Totta, in: C.Y. Li, P. Totta, P.S. Ho (Eds.), *Proceedings of the First International Workshop*, American Institute of Physics, Ithaca, New York, 1991, pp. 1–20.
- [2] R.E. Jones Jr., M.L. Basehore, *Appl. Phys. Lett.* 50 (1987) 725–727.
- [3] B. Greenebaum, A.I. Sauter, P.A. Flinn, W.D. Nix, *Appl. Phys. Lett.* 58 (1991) 1845–1847.
- [4] A.I. Sauter, W.D. Nix, *IEEE Trans. Comp. Hybrids Manuf. Technol.* 15 (1992) 594–600.
- [5] U. Burges, I. Eppler, W. Schilling, H. Schroeder, H. Trinkaus, in: S.H. Paul, J. Bravmen, C.Y. Li (Eds.), *Proceedings of the Third International Workshop*, American Institute of Physics, Stanford, CA, 1995, pp. 2–19.
- [6] T. Marieb, A.S. Mack, N. Cox, D. Gardner, X.C. Mu, in: H.J. Frost, M.A. Parker, C.A. Ross, E.A. Holm (Eds.), *Materials Research Society Symposium Proceedings*, vol. 403, 1996, pp. 639–644.
- [7] Y.L. Shen, *J. Appl. Phys.* 82 (1997) 1578–1581.
- [8] A. Gouldstone, Y.L. Shen, S. Suresh, C.V. Thompson, *J. Mater. Res.* 13 (1998) 1956–1966.
- [9] A. Wikström, P. Gudmundson, S. Suresh, *J. Appl. Phys.* 86 (1999) 6088–6095.
- [10] S.H. Rhee, Y. Du, P.S. Ho, *J. Appl. Phys.* 93 (2003) 3926–3933.
- [11] D. Ang, R.V. Ramanujan, in: A. Khor, R.V. Ramanujan, C.P. Ooi, J. Zhao (Eds.), *Third International Conference on Materials Processing for Properties and Performance*, vol. 3, Singapore, November 24–26, 2004, pp. 450–460.
- [12] P.J. McNally, J. Kanatharana, B.H.W. Toh, D.W. McNeill, A.N. Danilewsky, T. Tuomi, L. Knuuttila, J. Riikonen, J. Toivonen, R. Simon, *J. Appl. Phys.* 96 (2004) 7596–7602.
- [13] E.S. Ege, Y.L. Shen, *J. Elect. Mater.* 32 (2003) 1000–1011.
- [14] J.H. Zhao, W.J. Qi, P.S. Ho, *Microelectron. Reliab.* 42 (2002) 27–34.
- [15] L.T. Shi, K.N. Tu, *J. Appl. Phys.* 65 (1994) 1516–1518.
- [16] L.T. Shi, K.N. Tu, *J. Appl. Phys.* 77 (1995) 3037–3041.
- [17] A. Sekiguchi, J. Koike, K. Maruyama, *J. Appl. Phys.* 83 (2003) 1962–1964.
- [18] H. Niwa, H. Yagi, H. Tsuchikawa, *J. Appl. Phys.* 68 (1990) 328–333.
- [19] M.A. Korhonen, R.D. Black, C.-Y. Li, *J. Appl. Phys.* 69 (1991) 1748–1755.
- [20] J.A. King, *Materials Handbook for Hybrid Microelectronics*, Artech House, Boston, 1988.
- [21] J.M. Paik, H. Park, Y.C. Joo, *Microelectron. Eng.* 71 (2004) 348–357.
- [22] D. Ang, C.C. Wong, R.V. Ramanujan, *Thin Solid Films*, in press.
- [23] M. Hasunuma, H. Kaneko, A. Sawabe, T. Kawanoue, Y. Kohanawa, S. Komatsu, M. Miyauchi, *IEEE International Electron Devices Meeting, Technical Digest*, IEEE, Washington, DC, USA, 1989, pp. 677–680.
- [24] S. Kordic, R.A.M. Wolters, K.Z. Troost, *J. Appl. Phys.* 74 (1993) 5391–5394.
- [25] I.S. Yeo, P.S. Ho, *IEEE Proceedings of the International Reliability Physics Symposium*, IEEE, Dallas, TX, USA, 1996, pp. 131–138.
- [26] J.P. Lokker, G.C.A.M. Janssen, S. Radelaar, *Microelectron. Eng.* 50 (2000) 257–263.

- [27] D. Jawarani, H. Kawasaki, I.S. Yeo, L. Rabenberg, J.P. Stark, P.S. Ho, J. Appl. Phys. 82 (1997) 1563–1577.
- [28] P. Borgesen, J.K. Lee, R. Gleixner, C.Y. Li, Appl. Phys. Lett. 60 (1992) 1706–1708.
- [29] A. Sekiguchi, J. Koike, K. Maruyama, Mater. Trans. 43 (2002) 1633–1637.
- [30] H. Okabayashi, Mater. Sci. Eng. R11 (1993) 191–241.
- [31] J. Horváth, R. Birringer, H. Gleiter, Solid State Commun. 62 (1987) 319–322.
- [32] D. Gan, P.S. Ho, R. Huang, J. Leu, J. Maiz, T. Scherban, J. Appl. Phys. 97 (2005) 1–8.
- [33] <http://www.hkltechnology.com/data/0-Cu-lines.pdf>.
- [34] M.A. Korhonen, C.A. Paszkiet, C.Y. Li, J. Appl. Phys. 69 (1991) 8083–8091.
- [35] A. Sekiguchi, J. Koike, K. Maruyama, Appl. Phys. Lett. 83 (2003) 1962–1964.

List of Tables

Table 1	Materials properties
Table 2	Magnitude of hydrostatic stress gradients

List of Figures

- Fig. 1 Geometric model of copper damascene structure used in ANSYS.
- Fig. 2 A plot of hydrostatic stress in copper interconnect against aspect ratio. It is noted that Eshelby inhomogeneity model and numerical model predict a minimum point (indicated by arrows) at aspect ratio = 1.
- Fig. 3 A plot of hydrostatic stress vs. aspect ratio for copper interconnect, comparison between analytical, numerical and selected experimental data. It is noted that Eshelby inhomogeneity model and numerical model predict a maximum point (indicated by arrows) at aspect ratio = 1.
- Fig. 4 A plot of hydrostatic stress contours for copper interconnect of aspect ratio 0.1.
- Fig. 5 A plot of hydrostatic stress contours for copper interconnect of aspect ratio 1.
- Fig. 6 A plot of hydrostatic stress contours for copper interconnect of aspect ratio 10.
- Fig. 7 A plot of hydrostatic stress gradient (along the x -direction) contours for copper interconnect of aspect ratio 0.1.
- Fig. 8 A plot of hydrostatic stress gradient (along the y -direction) contours for copper interconnect of aspect ratio 0.1.
- Fig. 9 A plot of hydrostatic stress gradient (along the x -direction) contours for copper interconnect of aspect ratio 1.
- Fig. 10 A plot of hydrostatic stress gradient (along the y -direction) contours for copper interconnect of aspect ratio 1.
- Fig. 11 A plot of hydrostatic stress gradient (along the x -direction) contours for copper interconnect of aspect ratio 10.
- Fig. 12 A plot of hydrostatic stress gradient (along the y -direction) contours for copper interconnect of aspect ratio 10.
- Fig. 13 A plot of hydrostatic stress contours for copper interconnect (of periodic structure) of aspect ratio 1.
- Fig. 14 A plot of hydrostatic stress contours for copper (fully elastic) interconnect of aspect ratio 1.
- Fig. 15 A plot of hydrostatic stress gradient (along the x -direction) contours for copper (fully elastic) interconnect of aspect ratio 1.

Property and materials	<i>T</i> (K) for Si								
	293	393	422	477	533	589	644	723	
	<i>T</i> (K) for Cu								
				298	400	500	600	700	
α (10^{-6} K)									
Si	2.3	2.9	3.2	3.4	3.6	3.8	4.0	4.1	
Cu		–		16.5	17.6	18.3	18.9	19.5	
SiO ₂					1				
SiN					3.2				
Ta					6.5				
ν									
Cu					0.33				
Si					0.28				
SiO ₂					0.16				
SiN					0.27				
Ta					0.342				
Property and materials	<i>T</i> (K) for Cu								
				200	300	400	500	600	700
<i>E</i> (GPa)									
Cu		–	137	132	128	123	119	114	
Si					130				
SiO ₂					59				
SiN					220.8				
Ta					185.7				
Property and materials	<i>T</i> (K) for Cu								
				298	400	500	600	700	
σ_y (MPa)									
Cu		–	455	289	163	77	32		

Table 1

	Aspect ratio (MPa/ μm)		
	0.1	1	10
$ \text{d}\sigma_{\text{HS}}/\text{d}x $	715	452	8470
$ \text{d}\sigma_{\text{HS}}/\text{d}y $	1030	725	6250
$ \nabla\sigma_{\text{HS}} $	1254	854	10526

Table 2

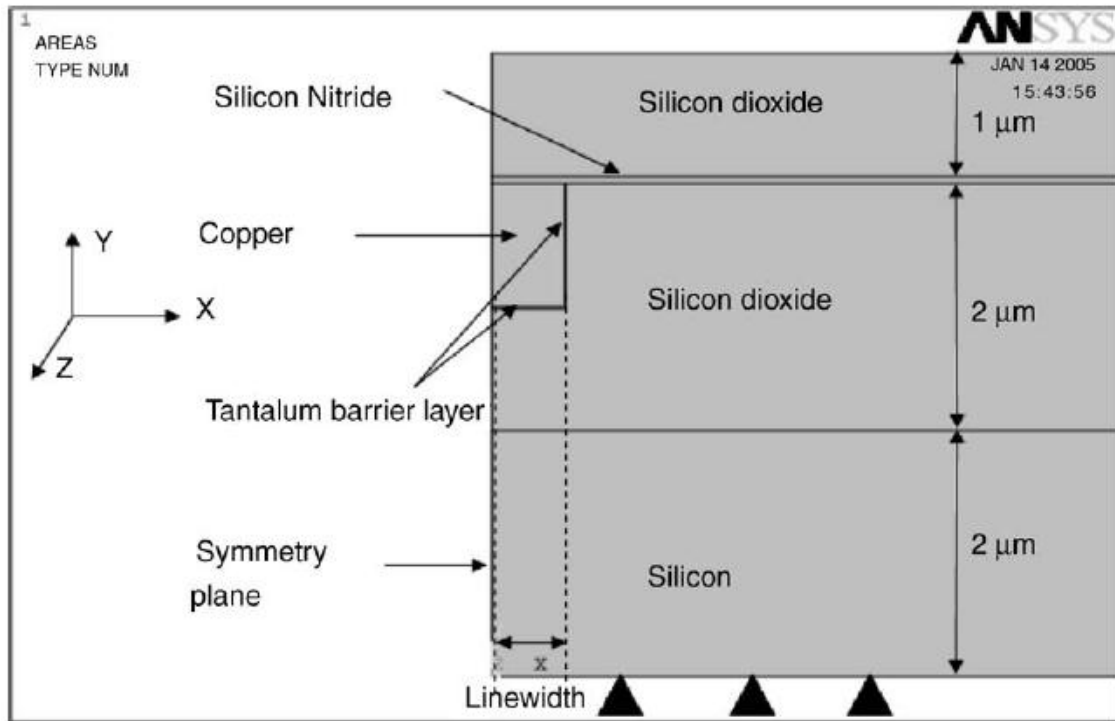


Fig. 1

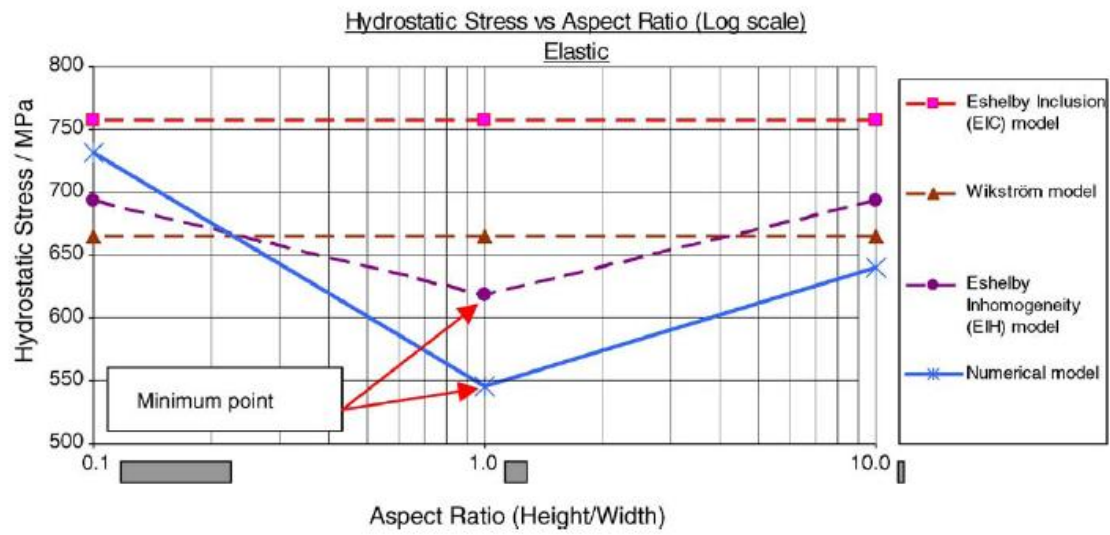


Fig. 2

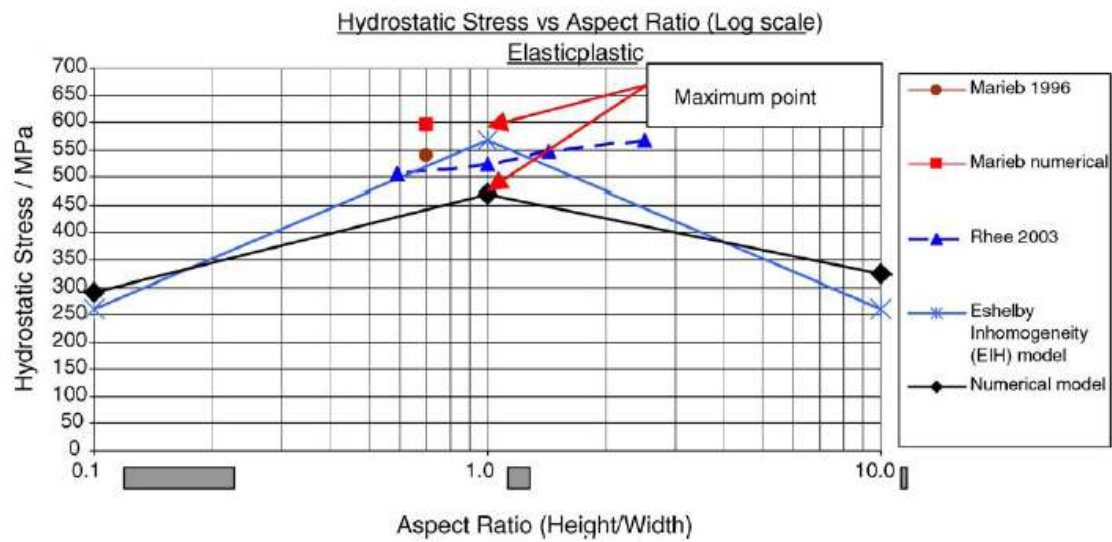


Fig. 3

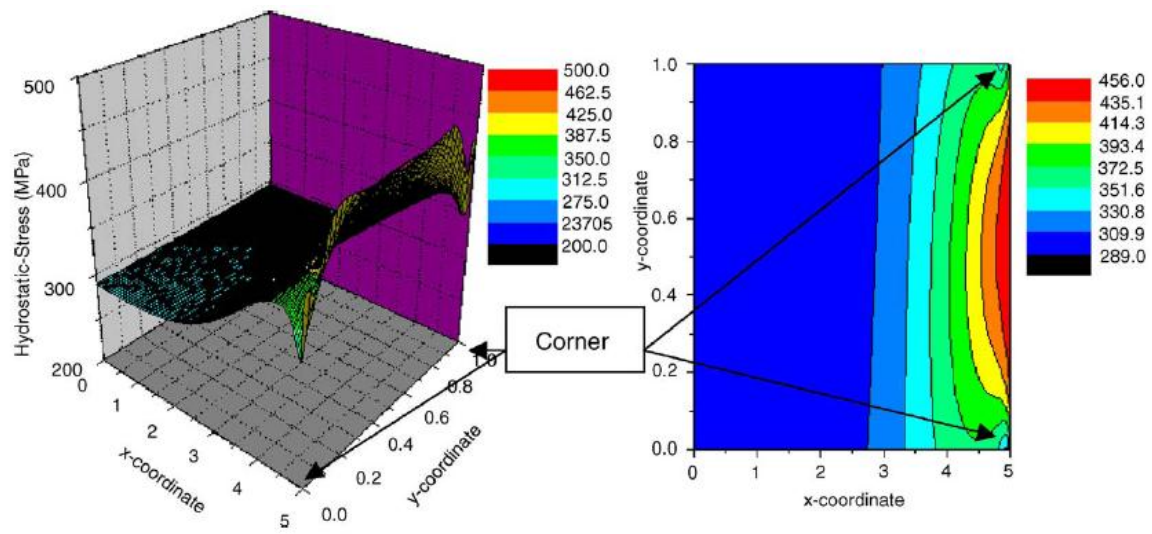


Fig. 4

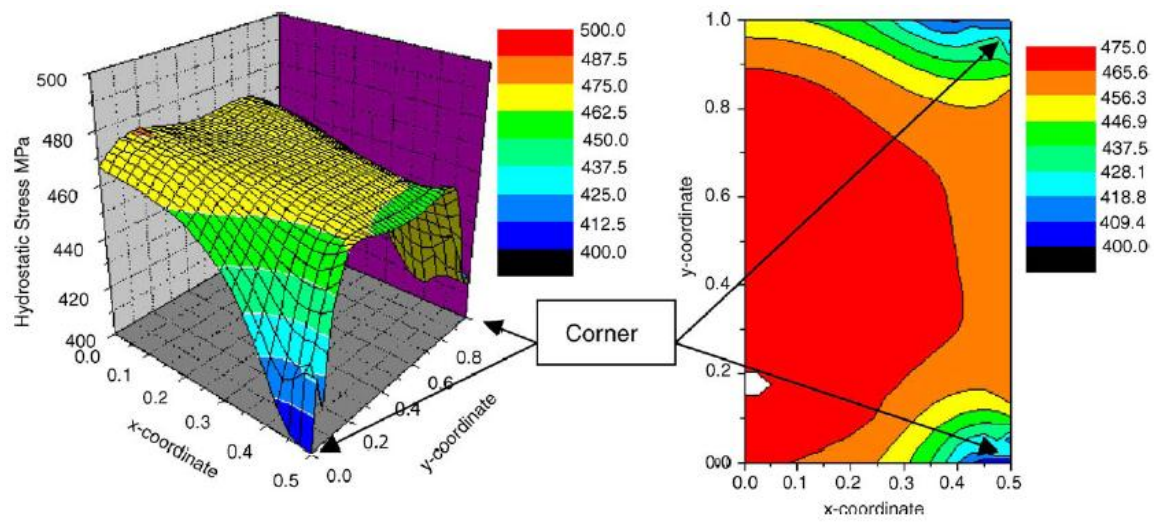


Fig. 5

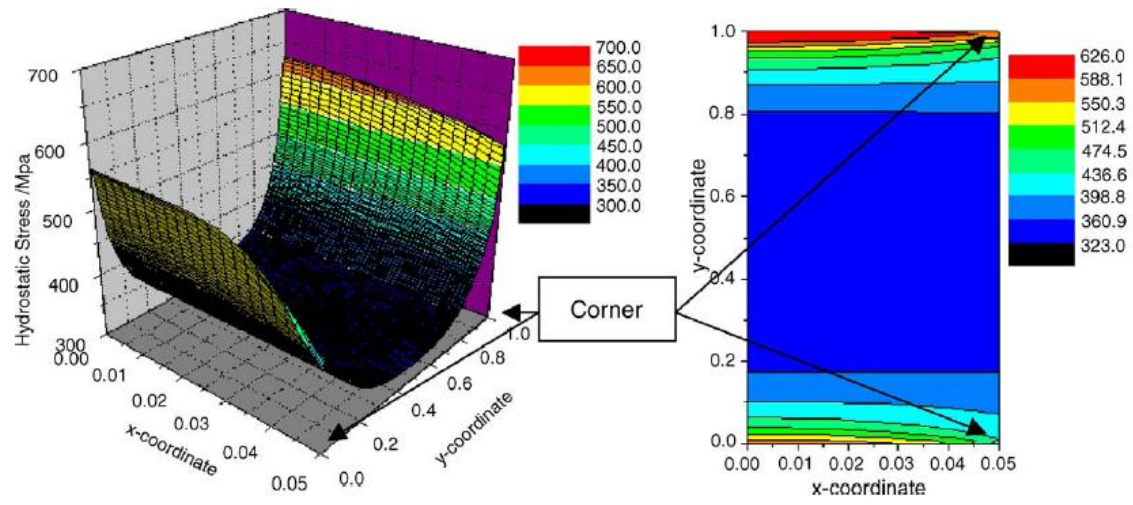


Fig. 6

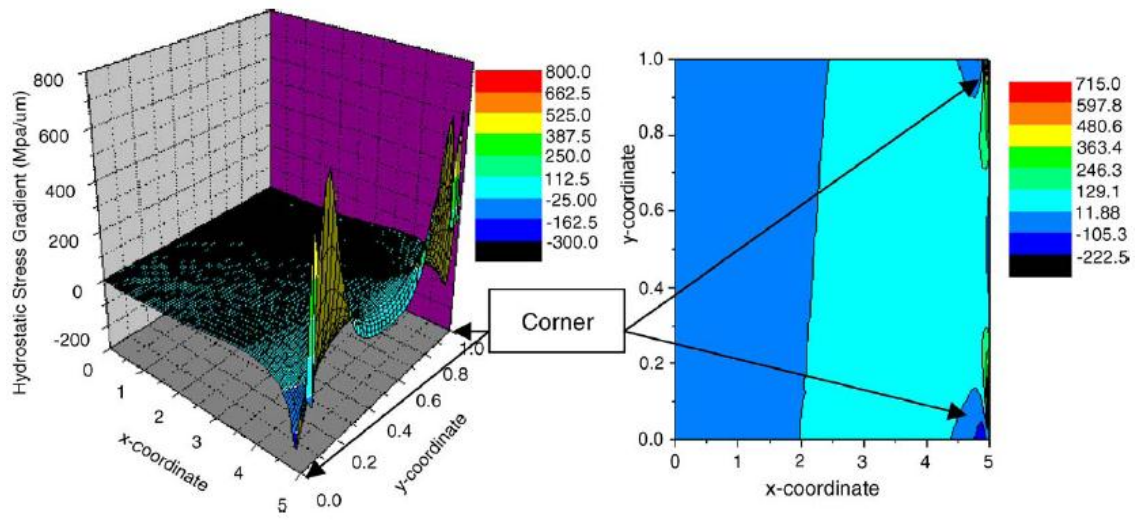


Fig. 7

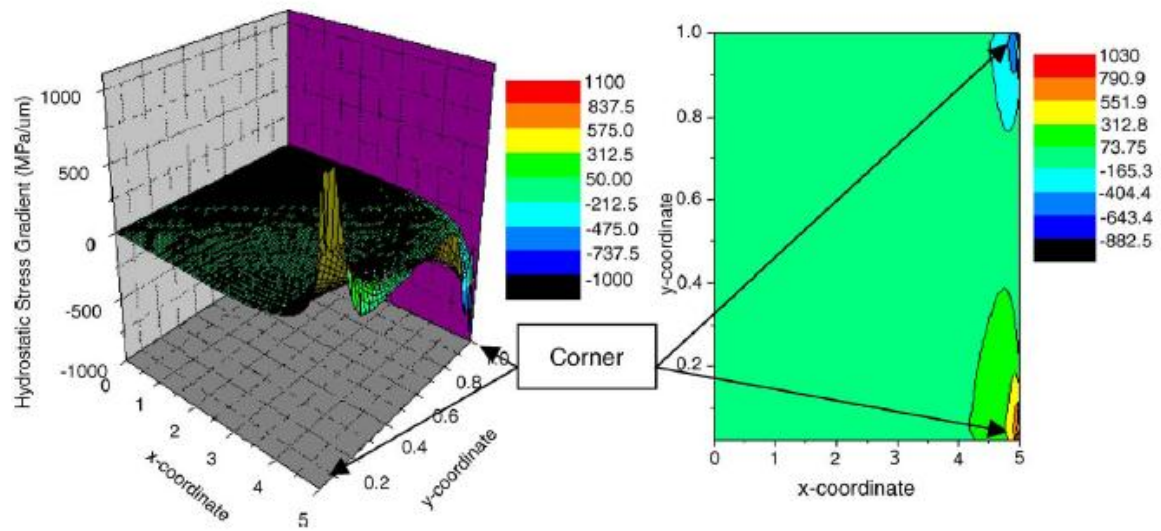


Fig. 8

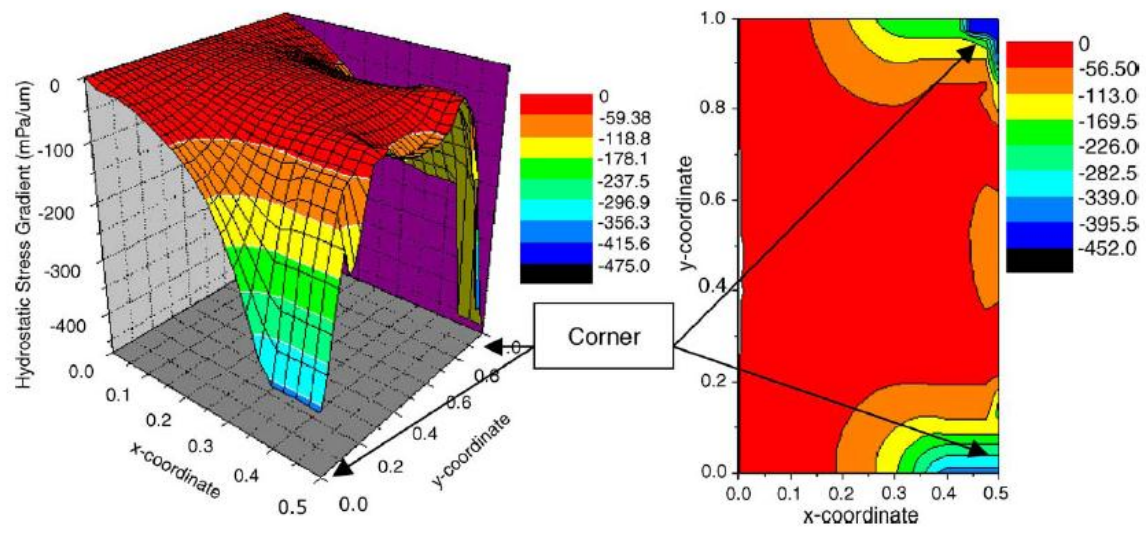


Fig. 9

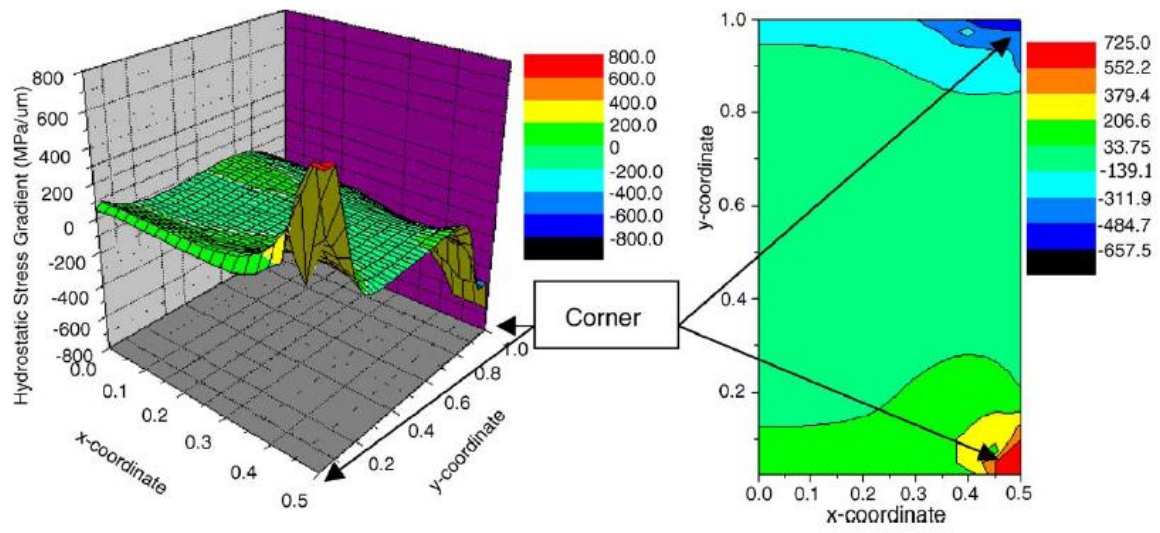


Fig. 10

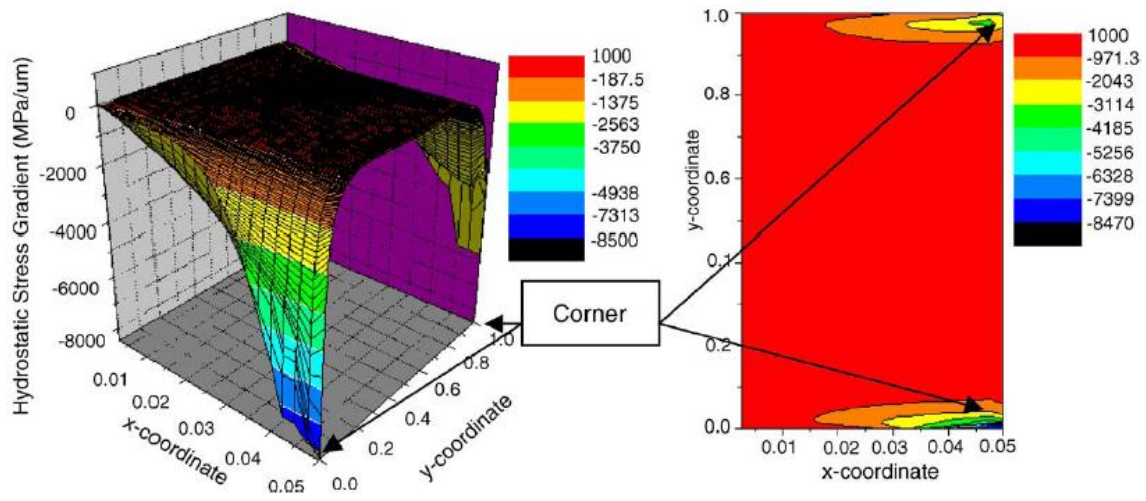


Fig. 11

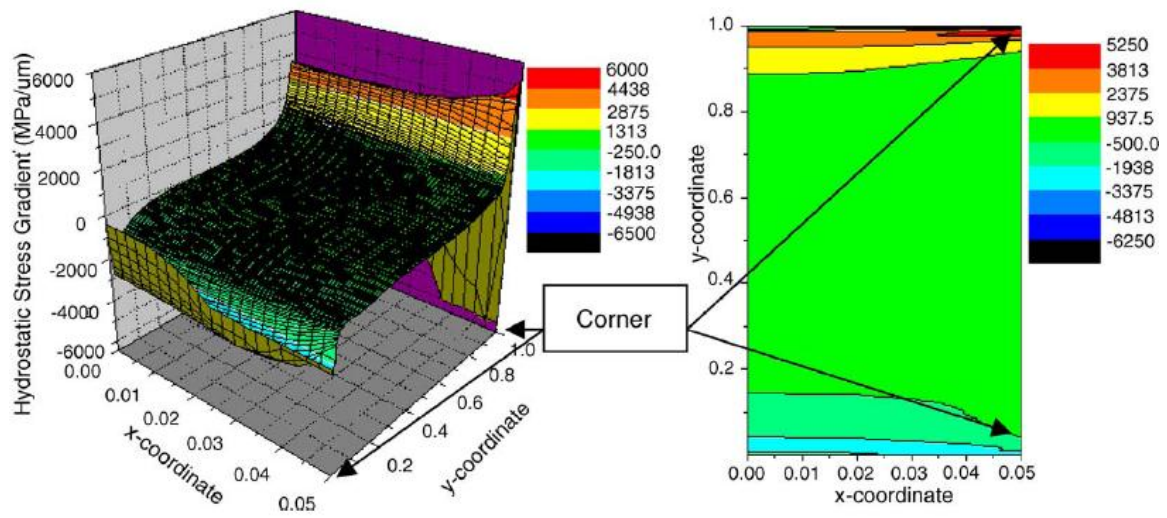


Fig. 12

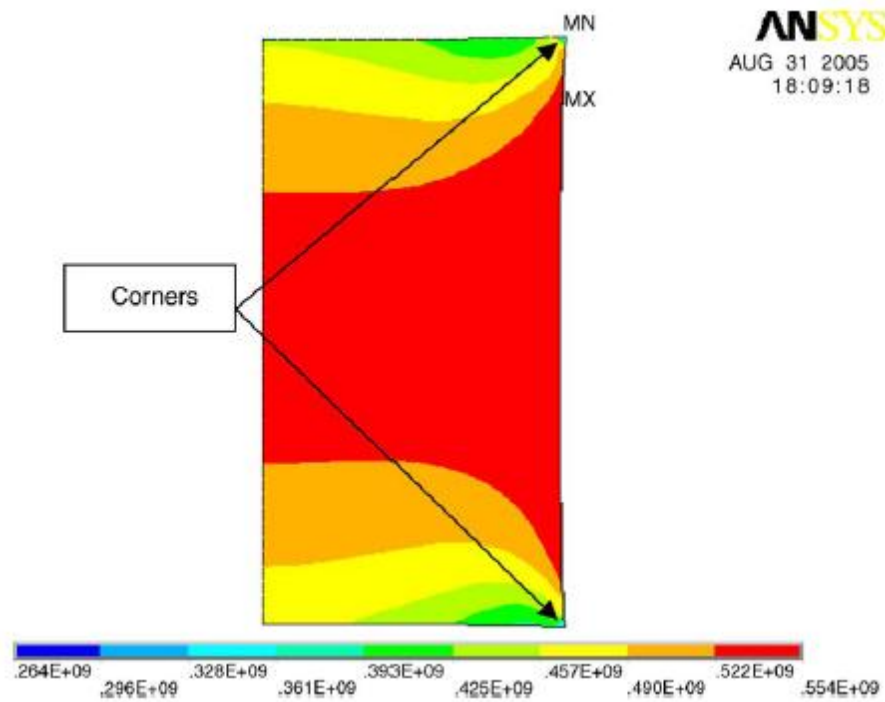


Fig. 13

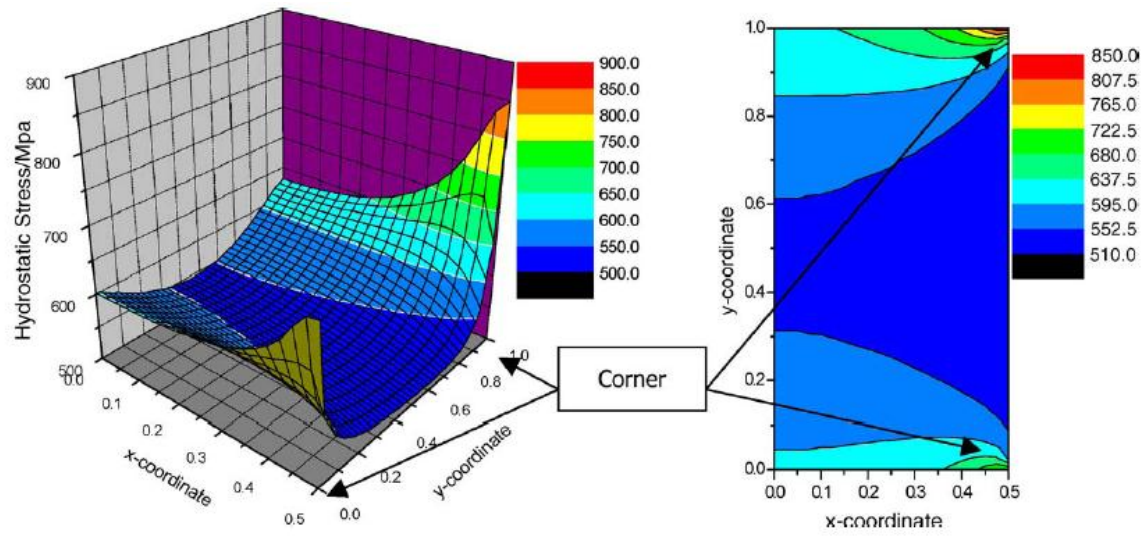


Fig. 14

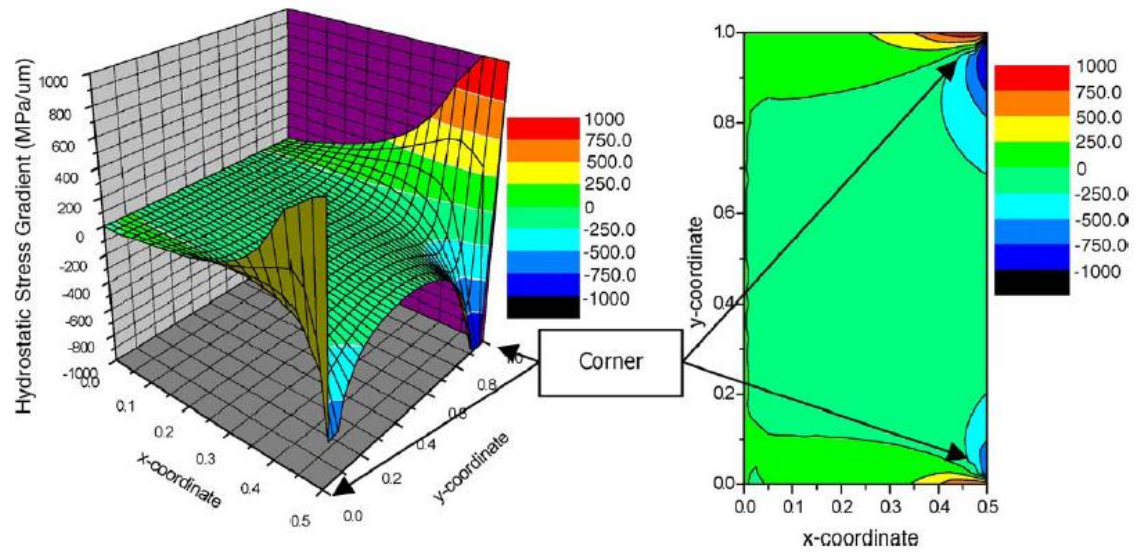


Fig. 15